Available online at www.sciencedirect.com
ScienceDirect
C. R. Physique 9 (2008) 857–873
COMPTES RENDUS PHYSIQUE
http://france.elsevier.com/direct/COMREN/

Recent advances in quantum dot physics / Nouveaux développements dans la physique des boîtes quantiques

Optical and electronic properties of quantum dots with magnetic impurities

Alexander O. Govorov

Department of Physics and Astronomy, Ohio University, Athens, OH 45701, USA

Available online 21 November 2008

Abstract

The article discusses some of the recent results on semiconductor quantum dots with magnetic impurities. A single Mn impurity incorporated in a quantum dot strongly changes the optical response of a quantum-dot system. A character of Mn-carrier interaction is very different for II-VI and III-V quantum dots (QDs). In the II-VI QDs, a Mn impurity influences mostly the spin-structure of an exciton. In the III-V dots, a spatial localization of hole by a Mn impurity can be very important, and ultimately yields a totally different spin structure. A Mn-doped QD with a variable number of mobile carriers represents an artificial magnetic atom. Due to the Mn-carrier interaction, the order of filling of electronic shells in the magnetic QDs can be very different to the case of the real atoms. The "periodic" table of the artificial magnetic atoms can be realized in voltage-tunable transistor structures. For the electron numbers corresponding to the regime of Hund's rule, the magnetic Mn-carrier coupling is especially strong and the magnetic-polaron states are very robust. Magnetic QD molecules are also very different to the real molecules. QD molecules can demonstrate spontaneous breaking of symmetry and phase transitions. Single QDs and QD molecules can be viewed as voltage-tunable nanoscale memory cells where information is stored in the form of robust magnetic-polaron states. ***To cite this article: A.O. Govorov, C. R. Physique 9 (2008).***

Résumé

Propriétes optiques et électroniques des boîtes quantiques dopées avec des impuretés magnétiques. Cet article traite des études récentes menées sur les boîtes quantiques dopées magnétiquement. Une impureté magnétique (comme le manganèse, Mn) incorporée dans une boîte quantique modifie radicalement la réponse optique de la nanostructure. Le caractère de l'interaction entre le Mn et les porteurs est très différent selon le matériau étudié : semiconducteurs II-VI ou III-V. Dans les boîtes quantiques à base de semiconducteurs II-VI, une impureté Mn influence uniquement la structure de spin d'un exciton. Dans les III-V, au contraire, la localisation spatiale d'un trou par l'impureté Mn peut jouer un rôle décisif sur la structure de spin des excitons confinés. Une boîte quantique dopée magnétiquement, contenant un nombre variable de porteurs représente un atome magnétique artificiel. Du fait de l'interaction porteurs-Mn, l'ordre de remplissage des couches électroniques dans la boîte quantique magnétique peut être très différent du cas des atomes réels. Les différentes espèces du « tableau périodique » des atomes magnétiques artificiels peuvent être réalisées par le biais de transistors contenant des boîtes quantiques magnétiques. Pour un nombre d'électrons confinés satisfaisant à la règle de Hund, le couplage magnétique entre les porteurs et les impuretés est particulièrement fort et les états de polarons magnétiques ainsi créés, particulièrement robustes. Les molécules de boîtes quantiques magnétiques sont également très différentes des molécules réelles. Elles présentent des effets de brisure de symétrie spontanée et des transitions de phase. Les boîtes quantiques magnétiques individuelles ainsi que les molécules formées par ces boîtes pourraient servir de nano-mémoires

E-mail address: Govorov@ohiou.edu.

1631-0705/$ – see front matter
doi:10.1016/j.crhy.2008.10.007

dans lesquelles l'information serait stockée sous la forme de polarons magnétiques robustes. ***Pour citer cet article : A.O. Govorov, C. R. Physique 9 (2008).***

Keywords: Quantum dot; Impurity; Exciton; Optical properties; Magnetic polaron

Mots-clés : Boîte quantique ; Impureté ; Exciton ; Propriétés optiques ; Polaron magnétique

1. Introduction

A quantum dot with magnetic impurities is a new type of nanostructure. A large number of recent experimental [1–12] and theoretical [13–37] papers on Mn-doped quantum dots (QDs) indicate growing interest in this type of nanomaterial. There are several interesting physical and device concepts associated with magnetic QDs and magnetic nanostructures. In semiconductors doped with magnetic impurities, the spins of static impurities interact through mobile carriers and can form a ferromagnetic state [38]. Since a carrier density in semiconductors is a voltage-tunable parameter, this ferromagnetic state also becomes controlled by the voltage [39]. A zero-dimensional nanostructure (i.e. a QD) can trap a small number of carriers and a carrier number can be controlled simply by a voltage [40]. By changing a voltage in a transistor structure with QDs, one can load electrons one by one [40]. When a single confined carrier (electron or hole) interacts with many magnetic impurities, it forms a new stable state, called a magnetic polaron [41]. It was shown theoretically that, in QDs, the magnetic-polaron states can be very stable and survive at relatively large temperatures [13,18,20,30]. Information in a single QD containing the magnetic polaron can be stored in the form of spin polarization and, therefore, such a QD can be considered as a nanoscale magnetic-memory element (see discussion in Section 3 and Figs. 10 and 11(a)). If a magnetic QD contains one or a few holes, the associated magnetic-polaron states are strongly anisotropic. Magnetic QDs as memory elements have some properties, that look very attractive for the technology: (i) small sizes; (ii) small number of carriers; (iii) anisotropy of magnetic energy; and (iv) voltage control of the number of carriers. Theory predicts interesting properties of QDs filled with few or several carriers. The "periodic" table of the magnetic QDs [20,21,27] can be very different to what we are used in the atomic physics. Regarding QDs with single Mn impurities, we should mention the great success in recent experiments on self-assembled CdTe and InGaAs QDs [1–4]. The presence of a single Mn atom in a QD was revealed optically through a characteristic fine structure of an exciton emission. For the first time, it became possible to study single magnetic impurities via optical means in detail. A character of the Mn–carrier interaction for an isoelectronic impurity (Mn in CdTe) and for an acceptor impurity (Mn in GaAs) are found to be very different. A QD "nano-lab" serves to localize an exciton in the vicinity of a single magnetic impurity and, in this way, the Mn–carrier interaction becomes amplified. Then, an optical emission spectrum of excitons in a QD reveals the properties of impurity–carrier interactions. For example, in the case of Mn impurities in bulk GaAs, previous macroscopic optical studies [42] were not able to reveal many important details of the impurity–carrier interaction. To conclude the introduction, we also note that a single Mn atom in a QD may serve as a qubit [19] since its spin is expected to have a long lifetime.

2. Models of a Mn impurity in quantum dots

Importantly, the character of an electronic state produced by a Mn impurity depends on the material system. In the II-VI semiconductors (such as CdTe or CdSe), a Mn atom forms an isoelectronic impurity [43], whereas in conventional III-V semiconductor materials (such as GaAs or InAs), a Mn gives rise to an accepter state. Therefore, physical models of QDs with Mn impurities can be very different for different material systems. The physical picture of magnetic isoelectronic impurity in II-VI QDs is relatively simple and should be considered first. In fact, the II-VI QDs with single Mn atoms can be considered as a model system, especially because of availability of detailed experimental results [1–3].

2.1. II-VI quantum dots: Exciton and Mn impurity

We now start with an isoelectronic Mn impurity in a II-VI QD. This impurity does not create an electric potential for carriers. However, it brings a spin-dependent exchange interaction between the Mn-impurity spin and mobile

carriers (electrons and holes). If an exciton (electron–hole pair) occupies a QD with a single Mn impurity, its spin Hamiltonian has a form [15]:

$$\hat{H}^{\text{spin}}_{\text{exciton}} = -\alpha\big(\vec{\hat{s}}_{\text{e}} \cdot \vec{\hat{I}}_{\text{Mn}}\big)\delta(r_{\text{e}} - R_{\text{Mn}}) - \frac{\beta}{3}\big(\vec{\hat{j}}_{\text{h}} \cdot \vec{\hat{I}}_{\text{Mn}}\big)\delta(r_{\text{h}} - R_{\text{Mn}}) + \hat{H}^{\text{e–h}}_{\text{exchange}}, \tag{1}$$

where $\vec{\hat{s}}_{\text{e}}$, $\vec{\hat{j}}_{\text{h}}$, and $\vec{\hat{I}}_{\text{Mn}}$ are the spin matrixes describing the conduction-band electrons, valence-band holes, and Mn impurity, respectively; $s_{\text{e}} = 1/2$, $j_{\text{h}} = 3/2$, and $I_{\text{Mn}} = 5/2$; the coordinates of electron and hole are r_{e} and r_{h}, respectively; the constants α and β are strengths of the contact carrier-Mn exchange interaction. Now we should make assumptions about electron and hole wave functions of a QD. We assume a disk-like self-assembled QD with dimensions $l_z < l_{x(y)}$, where l_z and $l_{x(y)}$ are the QD dimensions in the vertical (z) and in-plane (x, y) directions (Fig. 1(a)). Under these conditions, the envelope functions for a hole and an electron [$\varphi_{\text{e}}(r_{\text{e}})$ and $\varphi_{\text{h}}(r_{\text{h}})$] can be written as: $\varphi_\alpha(r) = B_\alpha \sin(\pi z/L)\psi_\alpha(x, y)$, where the index $\alpha = \text{e}, \text{h}$. We also can neglect the mixing between the heavy and light holes and include only the heavy-hole states. Then, the effective Hamiltonian becomes:

$$\hat{H}^{\text{spin}}_{\text{eff}} = \big\langle \hat{H}^{\text{spin}}_{\text{exciton}} \big\rangle = A_{\text{e}}\big(\vec{\hat{s}}_{\text{e}} \cdot \vec{\hat{I}}_{\text{Mn}}\big)\big|\varphi_{\text{e}}(R_{\text{Mn}})\big|^2 + A_{\text{h}}\big(\hat{j}_{\text{h},z} \cdot \hat{I}_{\text{Mn},z}\big) + \hat{H}^{\text{e–h}}_{\text{exchange}}, \tag{2}$$

where $A_{\text{e}} = -\alpha|\varphi_{\text{e}}(R_{\text{Mn}})|^2$ and $A_{\text{h}} = -\frac{\beta}{3}|\varphi_{\text{h}}(R_{\text{Mn}})|^2$. The important parameters for a Mn ion in CdTe are $\alpha N_0 = 0.29$ eV and $\beta N_0 = -1.4$ eV[13], where $N_0 = 15\ \text{nm}^{-3}$ is the spatial density of cations in the CdTe lattice. The signs of the exchange constants tell us that the electron and the Mn atom tend to form a ferromagnetic state, whereas the Mn–hole complex prefers an antiferromagnetic arrangement. Also one can note that the Mn–hole interaction in Eq. (2) is highly anisotropic. The electron–hole exchange interaction may also play an important role, especially in the absence of a Mn spin. Its operator is [44]

$$\hat{H}^{\text{e–h}}_{\text{exchange}} = a_z \hat{j}_{\text{h},z}\hat{s}_{\text{e},z} + b_z \hat{j}^3_{\text{h},z}\hat{s}_{\text{e},z} + b_x \hat{j}^3_{\text{h},x}\hat{s}_{\text{e},x} + b_y \hat{j}^3_{\text{h},y}\hat{s}_{\text{e},y}, \tag{3}$$

where the constants a_z and b_i ($i = x, y, z$) describe the isotropic and anisotropic exchange interactions, respectively. A complete and orthogonal set of spin wave functions involved in the Hamiltonian (2) is composed of 24 states

$$\Psi^{\text{exciton}}_{I_{\text{Mn},z}, j_{\text{h},z}, s_{\text{e},z}} = |I_{\text{Mn},z}\rangle \cdot |j_{\text{h},z}\rangle \cdot |s_{\text{e},z}\rangle,$$

$I_{\text{Mn},z} = \pm 5/2, \pm 3/2, \pm 1/2$, $j_{\text{h},z} = \pm 3/2$, and $s_{\text{e},z} = \pm 1/2$.

First, we neglect the electron–hole exchange interaction. Now we can see that the Mn–hole interaction plays the leading role ($|\beta/\alpha| \sim 5$) and we start with this interaction. For $\alpha = 0$, the spectrum of Eq. (2) has 6 lines and each line has a degeneracy $d = 4$. Six exciton energies are

$$E_{I_{\text{Mn},z}, j_{\text{h},z}, s_{\text{e},z}} = A_{\text{h}}(I_{\text{Mn},z} \cdot j_{\text{h},z}),$$

where the important constant $A_{\text{h}} > 0$ for CdTe-based QDs. Now we should comment on an emission intensity of the excitonic states. The bright exciton states are $\Psi_{\text{bright},\sigma_-} = |I_{\text{Mn},z}\rangle \cdot |-3/2\rangle \cdot |+1/2\rangle$ and $\Psi_{\text{bright},\sigma_+} = |I_{\text{Mn},z}\rangle \cdot |+3/2\rangle \cdot |-1/2\rangle$, emitting $\sigma_\mp$ photons. The other six states with $j_{\text{h},z} + s_{\text{e},z} = \pm 2$ are dark. In our electron–hole representation, a momentum of emitted photon $\sigma_{\text{photon}} = j_{\text{h},z} + s_{\text{e},z}$. We note that this simple 6-line structure of exciton in a QD with a single Mn ion was observed in the pioneering paper [1] (see Fig. 1(b)). Now we look at what happens if we start "switching on" the electron–Mn interaction and start "switching off" the hole–Mn coupling (see Fig. 2). First, when $A_{\text{h}} \gg A_{\text{e}}$, each peak becomes split. When $A_{\text{h}} \sim A_{\text{e}}$, the spectrum has 12 lines with approximately equal spacing between neighboring lines. When $A_{\text{h}} \ll A_{\text{e}}$, the spectrum acquires two groups of lines near the energies $E(J) = (A_{\text{e}}/2)(J(J+1) - s_{\text{e}}(s_{\text{e}}+1) - I_{\text{Mn}}(I_{\text{Mn}}+1))$ with $J = 2, 3$. For $A_{\text{h}} = 0$ and $A_{\text{e}} \neq 0$, the spectrum has two lines with energies $E(2)$ and $E(3)$ having degeneracy 5 and 7 (see Fig. 2). In the general case $A_{\text{e}} \neq 0$ and $A_{\text{h}} \neq 0$, only two dark states remain:

$$\left|I_{\text{Mn},z} = \frac{5}{2}\right\rangle \cdot \left|j_{\text{h},z} = \frac{3}{2}\right\rangle \cdot \left|s_{\text{e},z} = \frac{1}{2}\right\rangle \quad \text{and} \quad \left|I_{\text{Mn},z} = -\frac{5}{2}\right\rangle \cdot \left|j_{\text{h},z} = -\frac{3}{2}\right\rangle \cdot \left|s_{\text{e},z} = -\frac{1}{2}\right\rangle.$$

Inclusion of the electron–hole exchange interaction ($\hat{H}^{\text{e–h}}_{\text{exchange}}$) makes the spectrum irregular and, in principle, all states can emit photons [19]. The operator $\hat{H}^{\text{e–h}}_{\text{exchange}}$ mixes the exciton states $|j_{\text{h},z}\rangle \cdot |s_{\text{e},z}\rangle$ and $|-j_{\text{h},z}\rangle \cdot |-s_{\text{e},z}\rangle$. Also, in the presence of Mn–carrier interactions, this mixing makes all exciton states optically active. Fig. 3 shows how the exciton–Mn spectrum evolves as a function of the Mn-impurity position with respect to the QD center. For this figure,

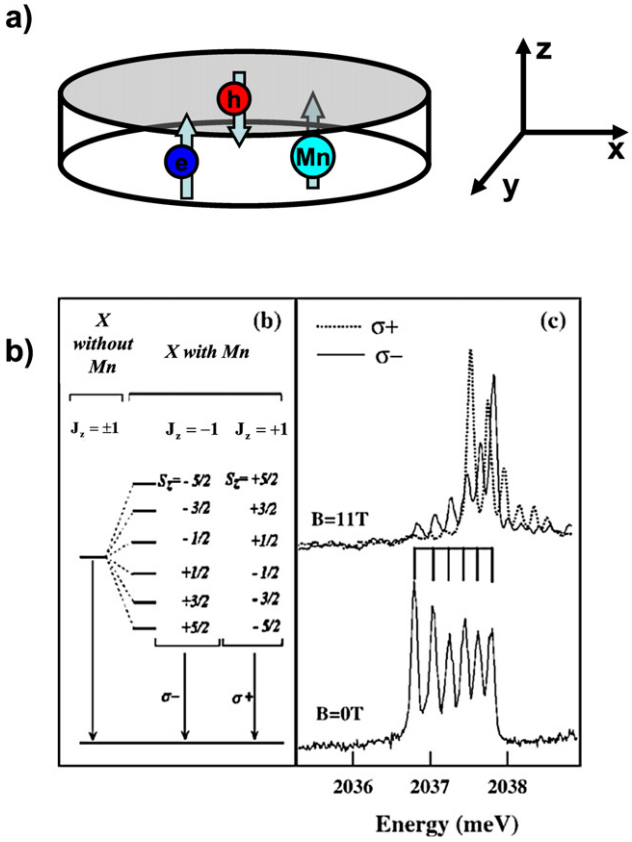

Fig. 1. (a) Geometry of a quantum dot with a magnetic impurity. (b) Diagram of inter-band transitions of an exciton in a QD without and with a Mn atom (left panel). Experimental spectrum of emission from a single QD with one Mn impurity. The graph (b) is reproduced from Ref. [1].

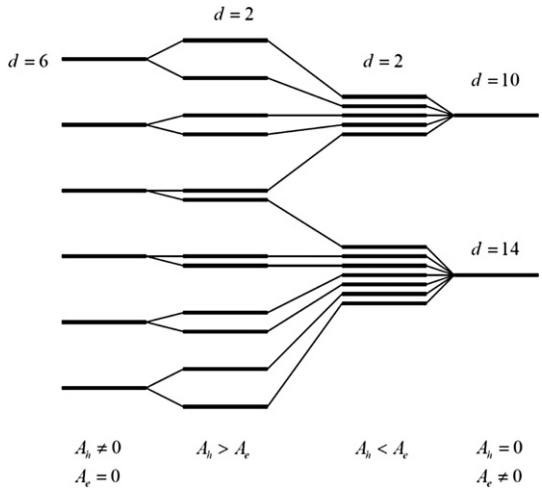

Fig. 2. Evolution of the exciton spectra as the Mn–hole and Mn–electron interactions become turned on or off. The symbol d denotes a degeneracy of a single level. For example, for $A_{\mathrm{e}} = 0$ and $A_{\mathrm{h}} \neq 0$, each level contains 6 states ($d = 6$).

we have chosen relatively strong anisotropic exchange couplings (b_i). For $R_{\mathrm{Mn}} \to \infty$, the spectrum has two bright states (upper lines) and two dark states (lower lines) [45]. Experimentally, more features of the Mn–exciton spectrum can be seen in the presence of an external magnetic field [1] and also for singly-charged excitons (X1− and X1+)[3].

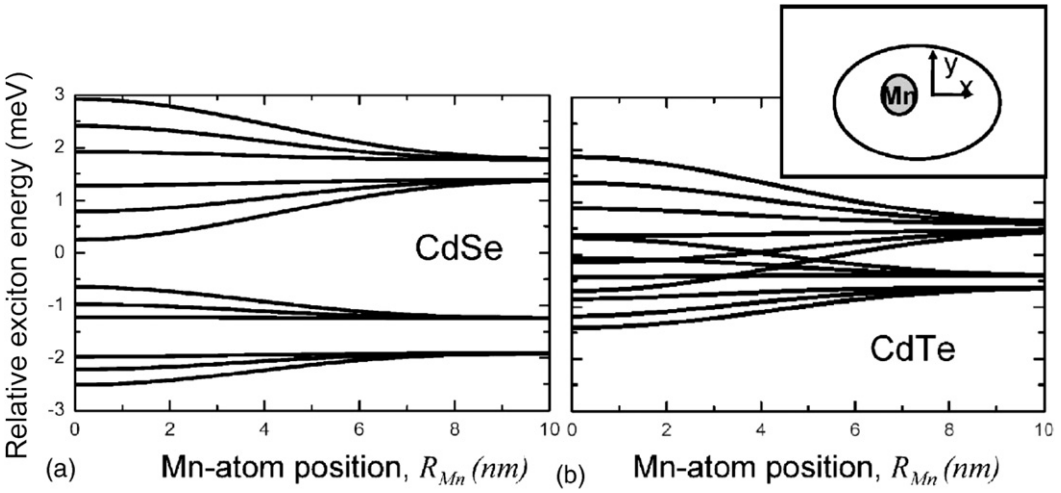

Fig. 3. Exciton energy spectrum as a function of the Mn-atom position for CdSe and CdTe QDs. The QD parameters can be found in Ref. [19]. Inset: geometry of the system. Reproduced from Ref. [19].

Then, to understand these features, all three terms in the spin Hamiltonian in Eq. (2) should be involved. We also should note that, in many experimental spectra [1–3], "dark" exciton states are weakly coupled to bright ones and can only be observed optically under specific conditions. This is also due to the fact that the first, isotropic term in Eq. (3) usually dominates the inter-band exchange interaction in the exciton and, therefore, the mixing between dark and bright states is relatively weak. To conclude this section, we should note that the papers [1–3] used spin Hamiltonians similar to Eq. (2). Prior to the publications [1–3,19], the paper [15] calculated an exciton spectrum for a spherical QD with one Mn spin, using the Luttinger Hamiltonian of the valence-band states.

2.2. III-V quantum dots: Exciton and Mn impurity

Now we will see that the excitonic picture for an InGaAs QD may be drastically different to that for the CdTe one. The optics of single InGaAs QDs is developed exceptionally well (see e.g. Refs. [45–48]). A next step can be a study of InGaAs QDs with magnetic impurities and this step has been made in the recent paper [4]. The main challenge with the Mn-doped InGaAs QDs is that a Mn impurity is not isoelectronic, i.e. it brings a strongly-bound acceptor state. This means that the orbital motion of carriers can be strongly perturbed due to the presence of a Mn impurity. Recall that for a Mn impurity in CdTe it is not the case. The Hamiltonian for the orbital and spin motions of an exciton in a III-V QD with a single Mn impurity should be constructed as [17]

$$\hat{H}_{\text{exciton}} = \hat{H}_{\text{h}}^{\text{QD}}(r_{\text{h}}) + \hat{H}_{\text{e}}^{\text{QD}}(r_{\text{e}}) + U_{\text{h}}^{\text{imp}}(r_{\text{h}}) + U_{\text{e}}^{\text{imp}}(r_{\text{e}}) + A_{\text{imp}}\big(\vec{\hat{j}}_{\text{h}} \cdot \vec{\hat{I}}_{\text{Mn}}\big)\delta(r_{\text{h}} - R_{\text{Mn}}) + \hat{H}_{\text{exchange}}^{\text{e–h}} + U_{\text{Coul}}(r_{\text{e}}, r_{\text{h}}), \tag{4}$$

where the operators

$$\hat{H}_{\text{h}}^{\text{QD}}(r_{\text{h}}) = \hat{T}_{\text{h}}(r_{\text{h}}) + U_{\text{h}}^{\text{QD}}(r_{\text{h}}),$$
$$\hat{H}_{\text{e}}^{\text{QD}}(r_{\text{h}}) = \hat{T}_{\text{e}}(r_{\text{e}}) + U_{\text{e}}^{\text{QD}}(r_{\text{e}})$$

describe the motion of electron and hole in the absence of Mn impurity. The $U_{\text{h(e)}}^{\text{imp}}$ are electrostatic spin-independent potentials acting on carriers by a Mn impurity; note that $U_{\text{h}}^{\text{imp}}$ is a localizing potential for the hole. The term $A_{\text{imp}}(\vec{\hat{j}}_{\text{h}} \cdot \vec{\hat{I}}_{\text{Mn}})\delta(r_{\text{h}} - R_{\text{Mn}})$ describes an important exchange interaction between a hole and Mn ion. For simplicity, we omit here the weaker electron–Mn exchange interaction (see discussion in Ref. [17]). The potential U_{Coul} is the Coulomb interaction; in many cases, U_{Coul} can be treated as a perturbation. Regarding the materials parameters, the Mn-acceptor binding energy in GaAs is $E_{\text{b}} = 112$ meV and, in InAs, it is lowered to 22 meV. Since InGaAs QDs may have a relatively low In content, the effective binding energy of hole can be close to 112 meV. In any case, E_{b} should be in

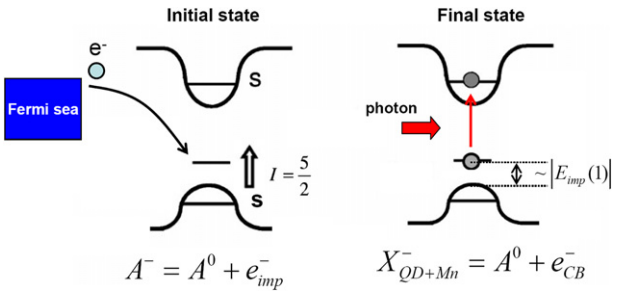

Fig. 4. Schematics of the optical absorption process in a QD with a Mn-acceptor level. The initial state is a charged Mn impurity $A^- = A^0 + e^-_{\rm imp}$ in which an additional electron, $e^-_{\rm imp}$, comes from the back contact (Fermi sea). The final state $X^-_{\rm QD+Mn}$ arises from A^- as a result of absorption of photon; in this inter-band optical transition, an impurity-bound electron is promoted to the s-state of a QD. Adopted from Ref. [17].

between 22 and 112 meV. Then, if we assume that a QD size is larger than a size of a bound-hole state, we should build the exciton wave functions differently. Typical sizes of electronic wave functions in self-assembled QDs are $l_{{\rm QD},z} \sim 3$ nm and $l_{{\rm QD},x(y)} \sim 4$–5 nm. A typical size of the Mn-accepter bound state within the envelope function approach [49] based on the Luttinger Hamiltonian is $l_{\rm Mn} \sim 0.6$ nm. We see that clearly $l_{\rm Mn} < l_{{\rm QD},i}$, where $i = x, y, z$. Therefore, we have chance to construct an exciton wave function as a product of a Mn-bound hole wave function and an electron wave function localized in a QD [17]:

$$\Psi^{\rm exciton}_{J_{\rm imp},J_{{\rm imp},z},s_{{\rm e},z}} = |J_{\rm imp};\, J_{{\rm imp},z}\rangle \cdot |s_{{\rm e},z}\rangle. \tag{5}$$

Here $|J_{\rm imp};\, J_{{\rm imp},z}\rangle$ is the set of Mn-bound hole wave functions of an uniform III-V crystal; the corresponding energies are $E_{\rm imp}(J_{\rm imp}) = E^0_{\rm imp} + \frac{\varepsilon}{2} J_{\rm imp}(J_{\rm imp}+1)$, where the exchange energy $\varepsilon \propto A_{\rm imp}$ [49]. Here $E_{\rm imp}(J) < 0$ corresponds to a bound state. In an isotropic crystal, the energy $E_{\rm imp}(J_{\rm imp})$ does not depend on the number $J_{{\rm imp},z}$. In a bulk crystal $\varepsilon > 0$ and, therefore, the ground state for the Mn-bound hole is a triplet with $J_{\rm imp} = 1 (J_{{\rm imp},z} = 0, \pm 1)$; its energy $E_{\rm imp}(1) = E^0_{\rm imp} + \varepsilon$. For excitons with lowest energies, we pick the Mn-bound hole states with $J_{\rm imp} = 1$. If the size of Mn impurity is smaller than QD dimensions and a Mn impurity is located in the center of a QD, the energy $|E_{\rm imp}(1)|$ is approximately a spacing between the impurity level and the potential maximum in the valence band (see Fig. 4). To find a fine structure of an exciton in a QD, we have to apply the QD potentials $U^{\rm QD}_{\rm h(e)}$ as perturbation to the states (5); note that we assume $l_{{\rm QD},i} \gg l_{\rm Mn}$. In addition, we should include the electron–hole exchange interaction. In Fig. 4, we show the schematics for the process of photon absorption from the initial ground state $A^- = A^0 + e^-_{\rm imp}$ to the exciton state $X^-_{\rm QD+Mn} = A^0 + e^-_{\rm CB}$; here A^0 is the neutral state of the Mn accepter (i.e. a hole bound to the attractive potential), $e^-_{\rm imp}$ is an electron occupying the Mn-accepter orbital, and $e^-_{\rm CB}$ is an electron in the conduction band state. We note that these states are the simplest states of the system and they are good as a starting point. The initial state $A^- = A^0 + e^-_{\rm imp}$ includes an electron coming from an electronic contact with a Fermi sea. Such electronic contact (back gate) is typical for voltage-tunable structures used in the current experiments with InGaAs QDs [4,47]. In the process of photon absorption (Fig. 4), a bound electron $e^-_{\rm imp}$ is promoted to the conduction band and becomes $e^-_{\rm CB}$. Therefore, the final states contain a Mn-bound hole. The QD potentials and electron–hole interaction split the triplet state of the bound hole ($J_{\rm imp} = 1$) and the exciton $X^-_{\rm QD+Mn}$ acquires a new fine structure (Fig. 5).

Interestingly, the only available experiment [4] on single InGaAs QDs with single Mn impurities presents the exciton lines related to the s–s transitions between electronic levels of a QD (Figs. 6 and 7). The corresponding exciton states identified in the spectra of Ref. [4] are $A^0 + X^0_{\rm QD}$ and $A^0 + X^-_{\rm QD}$. The transitions between the s-like electron state and the Mn-bound states (shown in Fig. 4) were not observed. The impurity hole state with $J_{\rm imp} = 1$ is treated in Ref. [4] as an "external" state to the exciton like in Ref. [17]. The interaction between an exciton in the s–s shell of a QD and the impurity hole state occurs via an exchange interaction, like in the model for CdTe QDs (see Eq. (4)). The simplest version of the interaction Hamiltonian can be constructed as

$$\hat{V}_{\rm exciton-impurity} = b_{\rm h} \cdot \hat{j}_{{\rm h,s-shell},z} \cdot \hat{J}_{{\rm imp},z} + b_{\rm e} \cdot \vec{\hat{s}}_{\rm e,s-shell} \cdot \vec{\hat{J}}_{\rm imp},$$

where the operator $\vec{\hat{J}}_{\rm imp}$ describes the hybrid angular momentum to the impurity-hole complex ($J_{\rm imp} = 5/2 - 3/2 = 1$); the s-shell state of hole in a QD is mostly formed from the heavy-hole component and, therefore, only

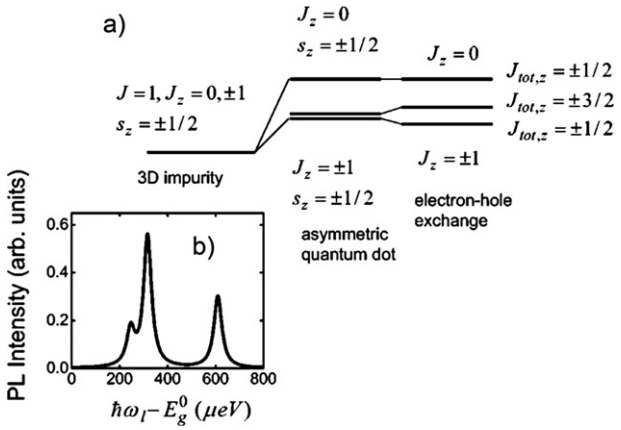

Fig. 5. (a) The lowest states of an exciton, $X^-_{\mathrm{QD+Mn}}$, in an InGaAs dot with a Mn impurity. (b) Calculated emission spectrum. Adopted from Ref. [17].

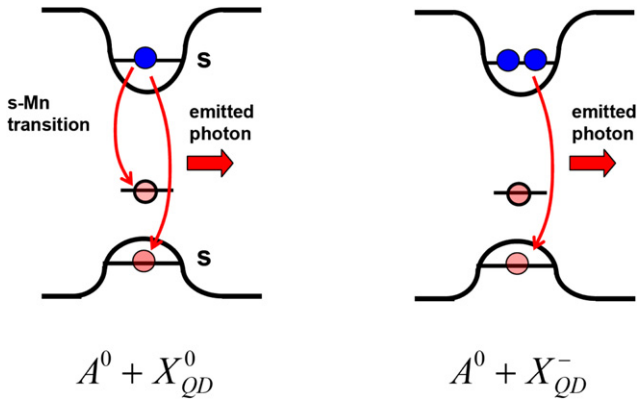

Fig. 6. Schematics of the optical emission processes in an InGaAs QD contacting a single Mn impurity. The s–s transitions were observed experimentally [4]. The s–Mn transition on the left panel was not recorded in Ref. [4].

z-components of momentum operators enter the equation for $\hat{V}_{\mathrm{exciton-impurity}}$. More details about the interaction operator can be found in Refs. [4,17,36]. The ability of this simple model to describe a set of magneto-photoluminescence spectra for $A^0 + X^0_{\mathrm{QD}}$, $A^0 + X^-_{\mathrm{QD}}$, and $A^0 + 2X^0_{\mathrm{QD}}$ in a QD with a single Mn is impressive. Theoretically, when we go from CdTe to InGaAs, the impurity spin momentum $I_{\mathrm{Mn}} = 5/2$ should be changed to $J_{\mathrm{imp}} = 1$. Of course, this essential simplification of the model requires a serious justification. Certainly, more theoretical studies are needed, using both the envelope-function and atomistic computational methods. Within the Luttinger–Hamiltonian model, the structure of localized states of holes in a QD with an impurity is quite complex; it depends on the characteristics of QD and impurity potentials ($U_{\mathrm{h}}^{\mathrm{QD}}$ and $U_{\mathrm{h}}^{\mathrm{imp}}$) [24,50]. For the state with two holes in the valence band, the character of localization becomes even more complex due to the Coulomb repulsion [51]. The model of Ref. [4] includes one hole strongly bound to a Mn impurity and another hole delocalized within extent of a QD (Fig. 6). This model is somewhat supported by the fact that the Mn-impurity in the bulk crystal seems to be unable to bind two holes. Therefore, in a QD system, the second hole may be delocalized within a QD. Recently, a more detailed theoretical description was developed involving several mechanisms of inter-particle interaction [36]. Here, in Fig. 8, we show a scheme of decay of $A^0 + X^-_{\mathrm{QD}}$, taken from Ref. [36].

As we already mentioned, the experiment [4] did not report the transitions between the s-like electron state and the Mn-bound states (shown in Fig. 4). It is likely that the s–Mn transitions have smaller intensities due to a relatively small overlap between the conduction-band electron wave function and the wave function of Mn-bound hole. In that sense, the Mn-levels were not seen directly in the experiments [4]; the presence of Mn was revealed through a fine structure of the conventional s–s transitions in a QD. It can be that the recently-developed absorption technique in

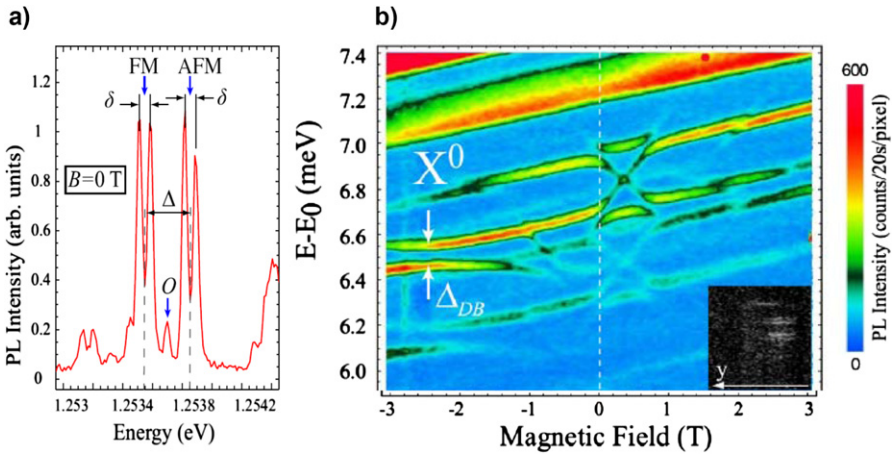

Fig. 7. Experimental magneto-photoluminescence spectra of the exciton $A^0 + X^0_{\mathrm{QD}}$ taken from the paper [4]. The lines FM, O, and AFM correspond to the different spin configurations of the exciton and Mn spins: ferromagnetic, "orthogonal", and antiferromagnetic. For more details, see Ref. [4]. Reproduced from Ref. [4].

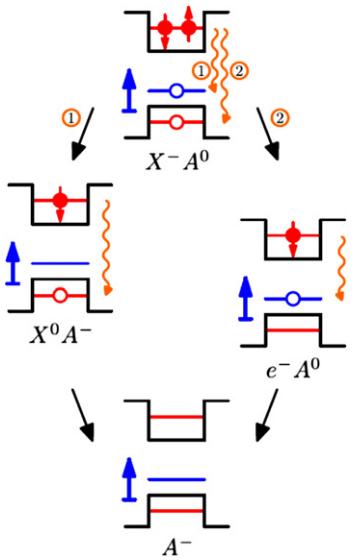

Fig. 8. Schematics of cascaded optical emission for $A^0 + X^-_{\mathrm{QD}}$ in an InGaAs QD with a Mn impurity from a theoretical paper [36]. Reproduced from Ref. [36].

single voltage-tunable QDs [47] can help to see directly the presence of Mn levels at lower photon energies around $E_{X^0_{\mathrm{QD}}} - \varepsilon_{\mathrm{hh}} - |E_{\mathrm{imp}}(1)|$, $E_{X^0_{\mathrm{QD}}}$ is the energy of the s–s transition in a QD and $\varepsilon_{\mathrm{hh}}$ is the heavy-hole quantization energy for the s-level (see the s–Mn transition in Fig. 6). More experimental studies are needed. It is likely that the main challenge is in the Mn-doped InGaAs material system.

As we already discussed in the introduction, the experiments with Mn-doped QDs permitted, for the fist time, to study in detail optical spectra of single magnetic impurities, such as a Mn impurity in CdTe or InGaAs. In that since, a QD system plays a role of "nano-lab".

2.3. Optical manipulation of spin of Mn impurity and spin relaxation processes

We now briefly consider optical manipulation of Mn spins and associated spin relaxation mechanisms in QDs. More description can be found in Refs. [19,52]. As an example, we consider the II-VI QDs. An important feature of

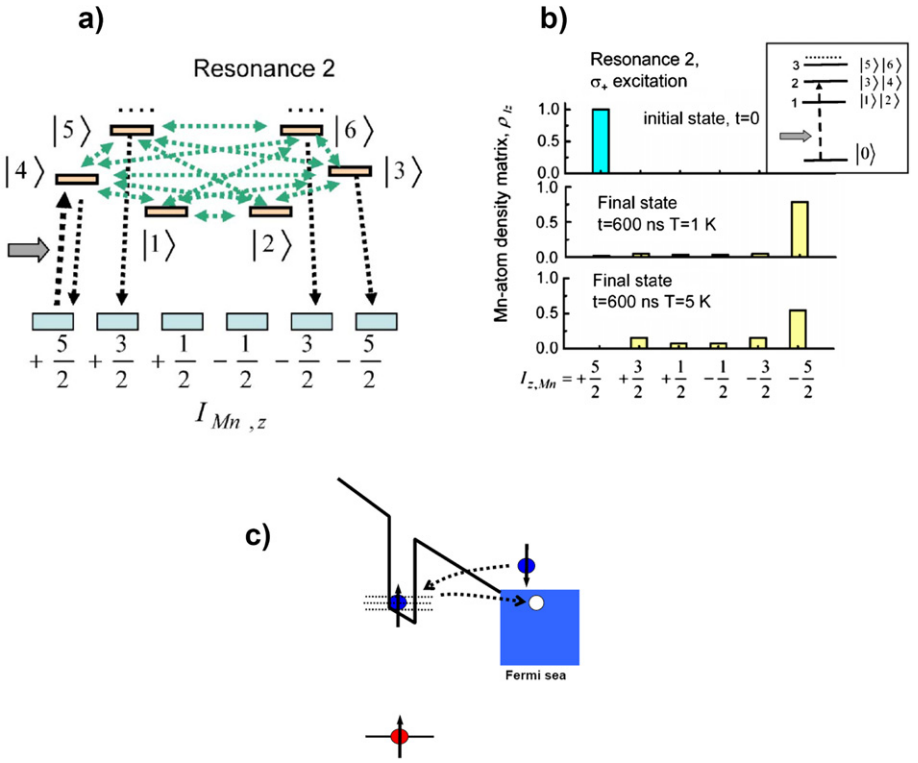

Fig. 9. (a) Schematics of pumping, relaxation, and PL processes in a QD with a Mn atom; the second level is resonantly excited; here we show only six lowest states. (b) Population of the Mn spin states at $t = 0$ and 0.6 ms for the resonant pumping into the second level (inset) at different temperatures. The initial spin state of Mn is $+5/2$. (c) Schematics of a spin-relaxation process in a voltage-tunable structure with an electronic back contact. Reproduced from Ref. [19].

a system with a few particles is a discrete spectrum. Then, selective excitation of states becomes possible. In a QD with a single Mn atom, the Mn–hole exchange interaction introduces a strong tendency to the cylindrical symmetry. Therefore, circularly-polarized emission is possible under pumping by circularly-polarized light in the absence of a magnetic field. Note that, in QDs without Mn impurities, emission at zero magnetic field is linearly polarized due to the anisotropic exchange interaction [45]. Optical spin orientation and associated circular emission from QDs with a single Mn were described theoretically in Ref. [19]. Experimentally, circularly-polarized emission was recorded from single CdTe QDs containing many Mn impurities [7,8,10]. These experiments [7,8,10] revealed rather interesting and complex dynamics of formation of magnetic polarons in single QDs. In particular, it was demonstrated that, using resonant circularly-polarized pumping, one can "write in" the magnetic polarization of a single QD in a sample; this magnetic-memory effect was observed as islands of long-lived magnetic polarization in a sample where each island corresponds to a single QD. In the simplest approach, the dynamics of an exciton in a QD with a single Mn impurity can be modeled using the rate equations [19] (Fig. 9(a)). It is important to identify the time scales of relaxation processes in the system. The longest time is associated with relaxation of the Mn spin in the absence of exciton, $\tau_{\mathrm{Mn}} \sim 1$–$100$ ms [53]. A radiative time of excitons is about 1 ns. Conveniently, a spin-relaxation time of the exciton–Mn complex ($\tau_{\mathrm{exc+Mn}}$) can be controlled by voltage via the co-tunneling (Kondo-like) processes and can be tuned in the range $\tau_{\mathrm{exc+Mn}} \sim 1$–$10$ ns [54]. The important inequality $\tau_{\mathrm{Mn}} \gg \tau_{\mathrm{exc+Mn}}$ allows us to manipulate the Mn spin using optical pulses [19]. An example is shown in Fig. 9(b). First, the Mn spin is prepared in a state $I_z = +5/2$. Then, using a selected resonance and σ_+-excitation, the initial Mn state ($I_z = +5/2$) becomes converted into the state $I_z = -5/2$. The preparation of the initial Mn state can be realized by observing a photon with certain energy and polarization [19]. Due to thermal activation processes, the spin manipulation at higher temperatures becomes less effective (Fig. 9(b)). This type of optical manipulation may be possible due to long spin lifetimes of an isolated Mn atom and a relatively short lifetime for a Mn–exciton complex ($\tau_{\mathrm{Mn}} \gg \tau_{\mathrm{exc+Mn}}$). Recently, the dynamics and photon-correlation functions of excitons in CdTe QDs with single Mn atoms were observed and theoretically modeled [52].

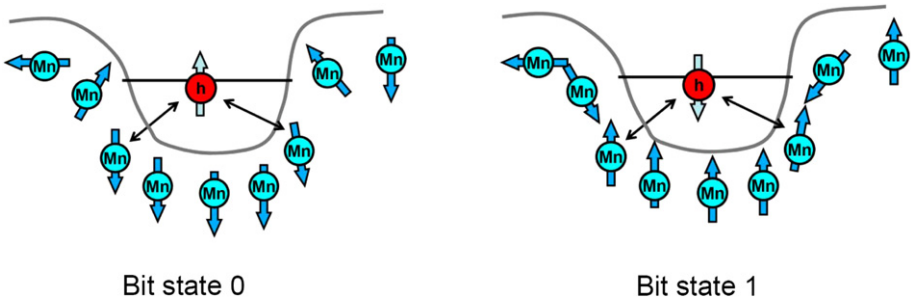

Fig. 10. Schematics of spin structure of a single hole orbiting in a Mn-doped QD. In a magnetic polaron based on the hole state in a self-assembled QD, two stable states exist with the hole momentums $j_z = \pm 3/2$. These states can be viewed as a classical bit with states 0 and 1. The arrows connecting the hole spin and Mn spins represent a carrier-mediated interaction; this interaction occurs between two stationary impurities via one orbiting hole.

Indeed, the rate-equation approach [19] is adequate to describe the exciton dynamics in experiments with Mn-doped QDs. Finally, we comment on the ability to manipulate the spins of Mn–exciton complexes using a voltage. Fig. 9(c) shows the schematics of spin relaxation when an exciton is placed nearby an electronic contact with a Fermi gas. Since a Fermi sea can "accommodate" any additional spin, an Mn–exciton complex can make spin-flip transitions relatively fast. We note here that the process in Fig. 9(c) is not a "real" tunneling process; this is a Kondo-like (or co-tunneling) process with two virtual tunneling events. The rate of spin flip transitions becomes greatly accelerated when the Fermi level of an electron contact is close to the electronic level in the exciton. In this way, the rate $\tau_{\text{exc+Mn}}$ can be tuned in a wide range $\tau_{\text{exc+Mn}} \sim 1$–$10$ ns [54]. We also note that, in optical experiments, spin-flip relaxation for single Mn spins and for Mn–exciton complexes may come from photo-generated carriers in a sample. This can be controlled through a power-dependence of spin-relaxation rates. Another mechanism of spin relaxation may be a direct carrier exchange between a QD and a wetting layer (or other electron reservoirs nearby a QD) [52].

3. Few-electron QDs with magnetic impurities

We start with the case of magnetic polarons. Magnetic polaron states become formed in a diluted magnetic semiconductor as a result of a spin–spin exchange interaction between single carriers and a large collection of localized impurities. Prior to appearance of QDs, the concept of magnetic polarons was introduced to describe an impurity-bound hole in a semiconductor with magnetic impurities [41]. In a magnetic polaron, a single mobile carrier interacts with many stationary impurities (Fig. 10). A carrier, orbiting in a QD, is able to polarize impurity spins within an extent of its wave function. While, outside a QD, impurity spins remain non-polarized (Fig. 10). Here, we focus on magnetic-polaron states coming from one or few holes in II-VI QDs. We also assume a voltage-tunable structure in which the number of holes is controlled by an electrical voltage [40] (Fig. 11(a)).

The hole states in self-assembled (disk-shape) QDs are strongly anisotropic because of a large splitting between heavy-hole and light-hole levels. Therefore, two magnetic-polaron states with $j_z = \pm 3/2$ (Fig. 10) are pretty stable and can be viewed as a classical bit. We note that magnetic-polaron lifetimes must be much longer than spin lifetimes of individual carriers (holes or electrons). The reason is in the strong Mn–carrier interaction that stabilizes the collective state of a charged carrier and many Mn spins.

A convenient way to describe a system composed of few carriers and many impurities is the mean-field approach [55,56]. For the case of a self-assembled (disk-like) QD with few holes, the mean-field Hamiltonian has a form [20]:

$$\hat{H}_{\text{eff}}^{\text{QD}} = \sum_n \left(\hat{T}^{(n)} + U_{\text{h}}^{\text{QD}}(r^{(n)}) - \frac{\beta}{3} x_{\text{Mn}} N_0 \cdot \hat{j}_z^{(n)} \cdot \bar{S}_{\text{Mn},z}\left(r^{(n)}\right) \right) + \hat{U}_{\text{Coul}}, \tag{6}$$

where $n = 1, 2, \ldots, N_{\text{h}}$ is the particle number, $r^{(n)}$ is the vector position of the nth hole. N_{h} is the total number of holes in a QD, x_{Mn} is the reduced spatial density of Mn impurities and $\bar{S}_{\text{Mn},z}(r)$ is the local Mn spin

$$\bar{S}_{\text{Mn},z}(r) = S B_S\left(S \frac{\beta/3 \cdot \bar{j}_z(r)}{k_{\text{B}}(T + T_0)} \right),$$

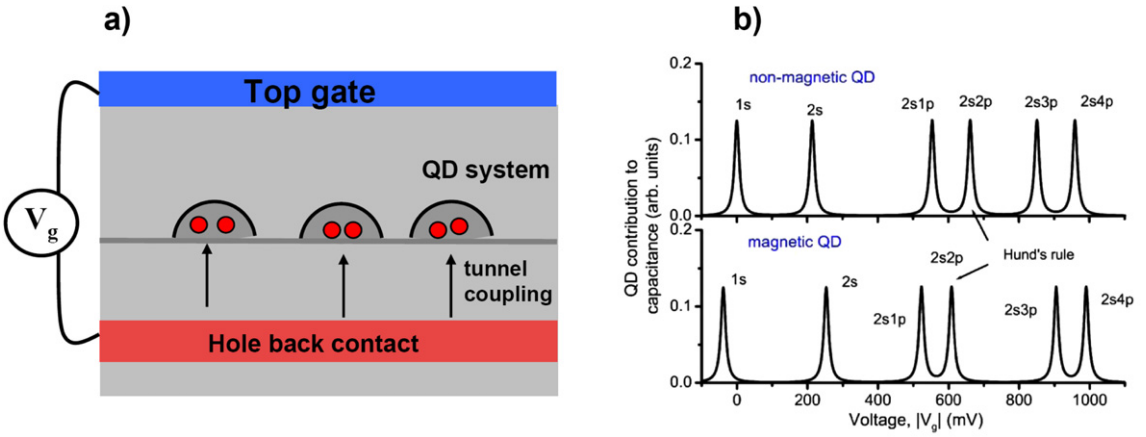

Fig. 11. (a) Transistor structure with magnetic QDs; the gate voltage controls the number of holes in the QD layer and therefore the magnetic state of the QDs. (b) The electrical capacitance of this structure can reveal the magnetic states of the QDs. Adopted from Ref. [20].

where $S = 5/2$, $\bar{j}_z(r) = \langle\Psi|\sum_n \hat{j}_z^{(n)}\delta(r^{(n)} - r^{(n)\prime})|\Psi\rangle$ is the local spin of holes, and $\Psi = \Psi(r^{(1)\prime}, r^{(2)\prime}, r^{(3)\prime}, \ldots)$ is the many-body wave function, $\hat{j}_z^{(j)}$ is the angular-momentum operator of a single heavy hole ($j_z = \pm 3/2$); T_0 is an effective temperature describing the antiferromagnetic Mn–Mn interaction. According the variational formalism, the solution for the effective mean-field non-linear Hamiltonian, $\hat{H}_{\text{eff}}^{\text{QD}}\Psi = E\Psi$, should be found as a minimum of the free-energy functional [30,55,56]:

$$F(\Psi) = \langle\Psi|\hat{H}_0|\Psi\rangle - \frac{\beta}{3}x_{\text{Mn}}N_0\langle\Psi|F_S\left(S\frac{\beta/3\,\bar{j}_z(r)}{k_{\text{B}}(T+T_0)}\right)|\Psi\rangle, \tag{7}$$

where $\hat{H}_0 = \sum_n(\hat{T}^{(n)} + U_{\text{h}}^{\text{QD}}(r^{(n)})) + \hat{U}_{\text{Coul}}$ and

$$F_S(u) = \left(\text{Ln}\left[\frac{\sinh\{(2S+1)u/2S\}}{(2S+1)\sinh\{u/2S\}}\right]\right)\Big/u,$$

and $u = S\beta/3\,\bar{j}_z(r)/(k_{\text{B}}(T+T_0))$. The minimum of the free energy yields the "ground" state at a given temperature. The stability and "robustness" of a Mn–hole magnetic polaron can be characterized by the total Mn–spin and by the magnetic binding energy:

$$S_{\text{Mn,tot}} = x_{\text{Mn}}N_0\int \text{d}r^3\,\bar{S}_z(r),$$

$$E_{\text{Mn–h,binding}} = -\frac{\beta}{3}x_{\text{Mn}}N_0\langle\Psi|B_S\left(S\frac{\beta/3\cdot\bar{j}_z(r)}{k_{\text{B}}(T+T_0)}\right)|\Psi\rangle.$$

The larger $|S_{\text{Mn,tot}}|$ and $|E_{\text{Mn–h,binding}}|$, the more stable a Mn–hole state against thermal and other fluctuations.

In a QD structure with electric gates, the number of carriers is controlled by a voltage (Fig. 11(a)). We now consider a QD with ideal cylindrical symmetry or with slightly-broken cylindrical symmetry so that the conventional picture of atom-like electronic shells is applied. The QD potential $U_{\text{h}}^{\text{QD}}(r) = u_{\text{h}}^{\text{QD}}(z) + v_{\text{h}}^{\text{QD}}(x,y)$, where $v_{\text{h}}^{\text{QD}}(x,y)$ is a harmonic-oscillator potential describing the in-plane motion in a QD. Single-hole states are taken as harmonic-oscillator wave functions and are described with the shell indices $(s, p, d, \ldots)$, like in real atoms. It is important to comment on our approach to treat the Coulomb interaction. We assume a QD with a relatively strong confinement and treat the Coulomb interaction as a perturbation. In other words, our assumption is that a Coulomb energy is less than an inter-level energy spacing of a QD. The role of the Coulomb interaction becomes very important in the case of partially-filled shells when we deal with degenerate orbital states. Then, the hole–hole Coulomb exchange interaction governs a spin configuration of holes and we should apply Hund's rule.

Since $\beta < 0$, the Mn–hole complex tends to form an antiferromagnetic arrangement at low temperatures. For a single hole ($N_{\text{h}} = 1$), the solution is simple: $|\Psi\rangle = |1_{s\uparrow}; 0_{s\downarrow}\rangle$ and $S_{\text{Mn,tot}} < 0$; here $|1_{s\uparrow}; 0_{s\downarrow}\rangle$ represents a state of a single hole in the s-orbital with the spin↑. The Mn–hole interaction leads to lowering of the total energy and the

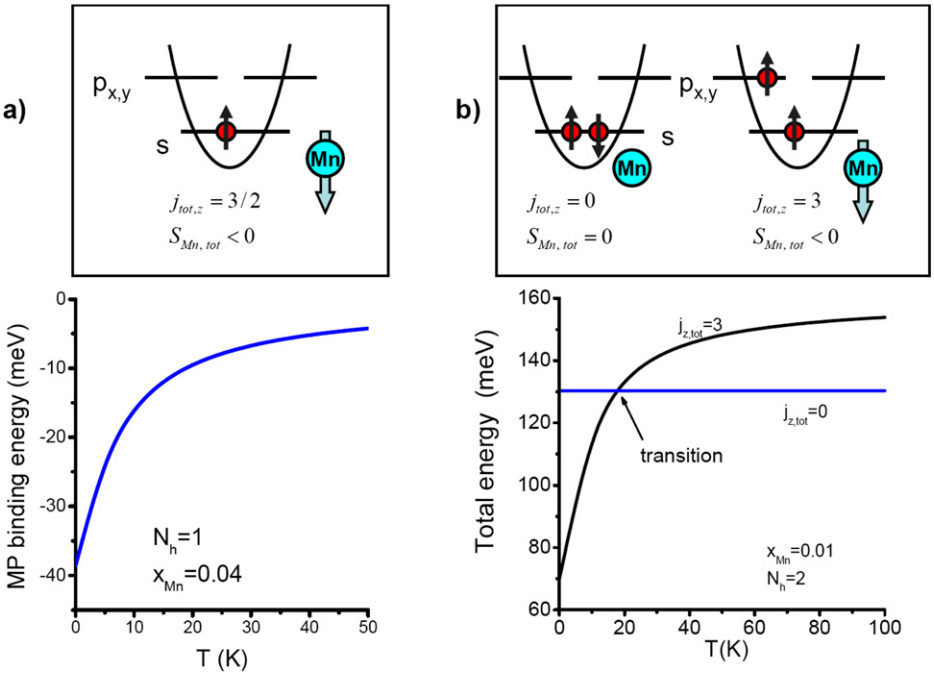

Fig. 12. (a) Upper panel: Spin configuration of one hole and a Mn subsystem. Lower panel: Calculated energy of a magnetic polaron with one hole. (b) Upper panel: Stable lowest-energy configurations of a QD with cylindrical symmetry and with two holes. The configuration $j_{\mathrm{tot},z} = 0$ and $S_{\mathrm{Mn,tot}} = 0$ is realized in the case of a relatively weak Mn–hole interaction (high temperature or small Mn density) and the state with $j_{\mathrm{tot},z} = 3$ and $S_{\mathrm{Mn,tot}} < 0$ corresponds to the system with a strong Mn–hole interaction (low temperature or high Mn density). Lower panel: The energies of the states $j_{\mathrm{tot},z} = 0$ and $j_{\mathrm{tot},z} = 3$ as a function of temperature; the ground state undergoes a transition with temperature. Adopted from Ref. [20].

formation of a magnetic polaron (Fig. 12(a)). Fig. 12(a) shows the spin configuration: the spin of hole and the Mn spins are opposite. We note that the paper [13] contains similar calculations performed for a single hole in a spherical QD. In a two-hole system, the lowest state is less trivial. The system with $N_{\mathrm{h}} = 2$ can undergo transition from the state with $j_{\mathrm{tot},z} = 0$ to a state $j_{\mathrm{tot},z} = 2 \cdot 3/2 = 3$, where $j_{\mathrm{tot},z} = \langle \Psi | \sum_n \hat{j}_z^{(n)} | \Psi \rangle$. This transition can occur with lowering the temperature (see Fig. 12(b)). The corresponding configurations are $|\Psi_{j_{\mathrm{tot},z}=0}\rangle = |1_{s\uparrow}; 1_{s\downarrow}; 0_{p_x\uparrow}; 0_{p_y\downarrow}; 0_{p_x\uparrow}; 0_{p_y\downarrow}\rangle$ and $|\Psi_{j_{\mathrm{tot},z}=3}\rangle = |1_{s\uparrow}; 0_{s\downarrow}; 1_{p_x\uparrow}; 0_{p_y\downarrow}; 0_{p_x\uparrow}; 0_{p_y\downarrow}\rangle$; here we include into our consideration only the s- and p-shells. In the low-temperature state $j_{\mathrm{tot},z} = 3$, the Mn–spin polarization is enhanced ($S_{\mathrm{Mn,tot}} < 0$) and for the high-temperature state with a closed s–shell $S_{\mathrm{Mn,tot}} = 0$. This transition can also occur at a fixed temperature as we vary other parameters determining the Mn–hole interaction, such as x_{Mn}, β, or l_{QD}, where l_{QD} is a QD size. The physical reason for the transition $j_{\mathrm{tot},z} = 0 \to j_{\mathrm{tot},z} = 3$ is the lowering of the total free energy due to a formation of a robust magnetic-polaron state. The condition for the ground-state transition is $F(\Psi_0) = F(\Psi_3)$ or

$$E_{j_{\mathrm{tot},z}=3} - E_{j_{\mathrm{tot},z}=0} = \left| \frac{\beta}{3} x_{\mathrm{Mn}} N_0 \langle \Psi_{j_{\mathrm{tot},z}=3} | F_S \left(S \frac{\beta/3 \cdot \bar{j}_z(r)}{k_{\mathrm{B}}(T + T_0)} \right) | \Psi_{j_{\mathrm{tot},z}=3} \rangle \right|,$$

where $E_{j_{\mathrm{tot},z}} = \langle \Psi_{j_{\mathrm{tot},z}} | \hat{H}_0 | \Psi_{j_{\mathrm{tot},z}} \rangle$ are the pure electronic energies of the corresponding states. Note that, if we lower x_{Mn} from the value in Fig. 10, the transition does not occur at any temperature. Therefore, for a sufficiently small Mn–hole interaction (for example, for $x_{\mathrm{Mn}} < x_{\mathrm{Mn,crit}}$ or for $T > T_{\mathrm{crit}}$), the shell filling in a "periodic table" for an artificial magnetic atom (QD) occurs in the conventional manner (Fig. 13(a)). Probably the most interesting observation is a strong enhancement of a magnetic-polaron binding energy in the regime of Hunds's rule, $N_{\mathrm{h}} = 4$ and 9 (Fig. 13). According to Hund's rule, a wave function with a maximum spin gives a ground state of a few-particle system; this happens due to the hole–hole exchange interaction. For the states with the maximum total hole momentum (half-filled shells at $N_{\mathrm{h}} = 4$ and 9), the magnitudes of binding energy and Mn–spin polarization are at maximum. Inset of Fig. 13(b) shows the polaron-enhancement effect for the p-shell at $N_{\mathrm{h}} = 4$. When carriers occupy the d-shell ($7 \leqslant N_{\mathrm{h}} \leqslant 12$), we also have the maximum polaron binding at $N_{\mathrm{h}} = 9$ [20]. To conclude, we see that, in a magnetic QDs, the hole–hole exchange coupling (Hund's rule) and Mn–hole exchange interaction enhance each other, creating especially

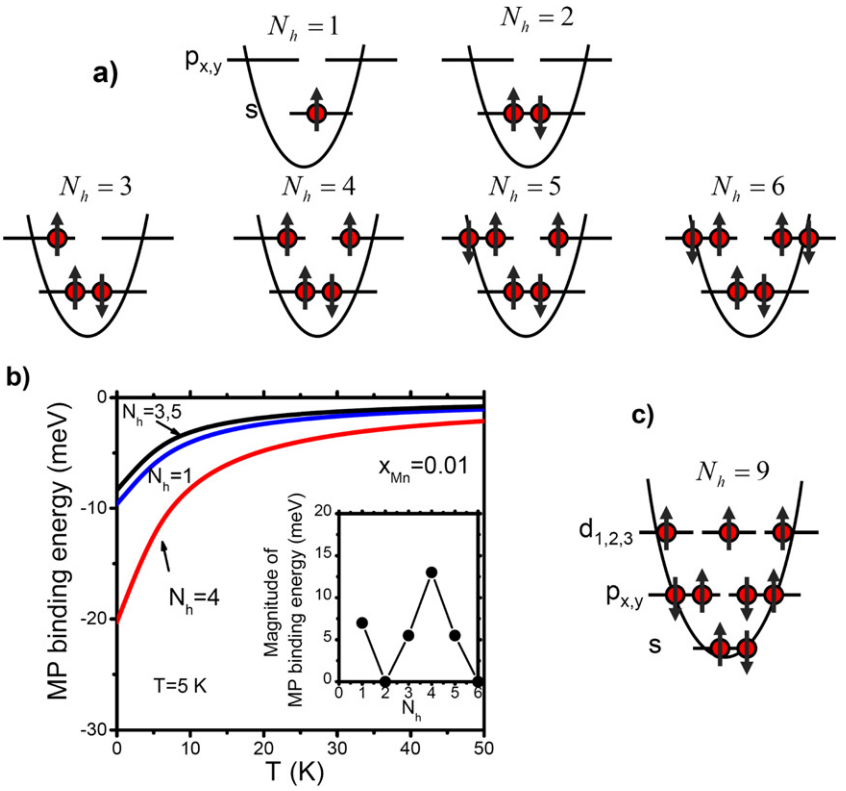

Fig. 13. (a) A periodic table for an artificial magnetic atom (of course, we mean a QD) for the states $N_{\rm h} = 1$–6. The graph shows stable lowest-energy configurations of a cylindrical QD if the Mn–hole interaction is relatively weak (or the QD confinement is strong enough). The state with $N_{\rm h} = 4$ is constructed according to Hund's rule. (b) Calculated binding energy of a magnetic polaron for various charged states of a QD. The binding energies for the states with completely filled shells ($N_{\rm h} = 2, 6$) are zero in our approach. (c) Lowest-energy configuration for $N_{\rm h} = 9$ in the regime of Hund's rule; again this configuration represents a ground state if the Mn–hole interaction is not very strong. Reproduced from Ref. [20].

"robust" magnetic-polaron states with half-filled shells with $N_{\rm h} = 4, 9, \ldots$. Regarding the filling of degenerate states (e.g. p_x and p_y orbitals) in magnetic QDs described by a non-linear Hamiltonian (6), one can see discussion in the paper [20].

One efficient method to study quantum states of QDs is a capacitance spectroscopy. In Fig. 11(b) we show the calculated capacitance of magnetic QDs with the normal order of filling of electronic shells; this corresponds to a relatively small Mn concentration when ground-state transitions (like the spin transition for $N_{\rm h} = 2$ shown in Fig. 12) do not occur. The formation of magnetic-polaron states manifests in the capacitance spectra $C(V_g)$ through positions and spacing between peaks. Experimentally, the magnetic-polaron energy contribution to the position of capacitance peaks can be revealed by varying the temperature. We note that, in strongly-doped QDs, the order of the capacitance peaks can be different reflecting magnetic ground-state transitions.

The above results are valid for QDs with a relatively strong confinement. In this case, we can treat Coulomb interaction as a perturbation. A much more complex method, applicable also to QDs with a weak confinement, was used recently in Refs. [27,28]. The authors of Refs. [27,28] employed the Kohn–Sham equations and the local spin density approximation; the Mn-subsystem was again described using the mean-field approach. Fig. 14 shows the results [27]. We can see how the shell filling and Coulomb interaction affect magnetic-polaron states with different number of electrons, N. The confining potential in these calculations was taken as a 2D Gaussian function which lifts partially degeneracy of the d-shell (see Fig. 14(a)). This lifted degeneracy of single-particle states is the reason for the antiferromagnetic-to-ferromagnetic transition for $N = 8$ (Fig. 14(c)). Another version of the mean-field theory for several electrons confined in a quantum box was used in an early paper [18]. Importantly, the authors of Ref. [18] found that the typical temperatures for ferromagnetic ordering in QDs are much higher than those in bulk. Another result was that the magnetization of a QD depends dramatically on the parity of the number of electrons in the dot,

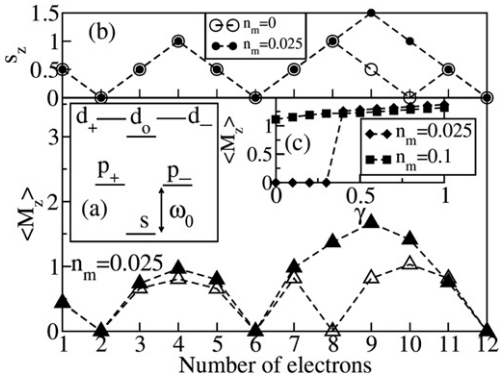

Fig. 14. Main panel: The averaged Mn-magnetization per unit area $\langle M_z \rangle$ as a function of number of electrons N at $T = 1$ K and Mn-density $n_m = 0.025$ nm^{-3}, for non-interacting ($\gamma = 0$, empty triangles) and interacting ($\gamma = 1$, filled triangles) electrons. The ground state of the QD changes between ferromagnetic and antiferromagnetic arrangements as a function of N. In particular, the Coulomb interaction creates a transition from antiferromagnetic to ferromagnetic state for the case of $N = 8$. (a) The single-particle levels of a 2D Gaussian potential. (b) The z-component of the total spin of electrons as a function of N for $\gamma = 1$. (c) Antiferromagnetic-ferromagnetic transitions for $N = 8$ as a function of the Coulomb interaction, γ. Reproduced from Ref. [27].

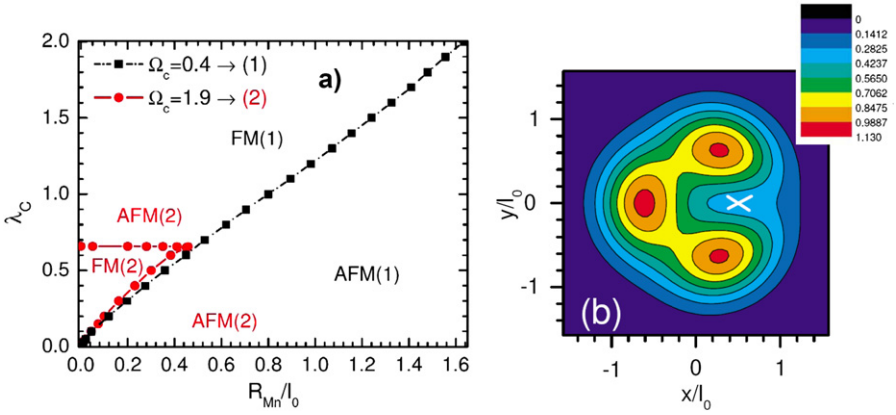

Fig. 15. (a) Phase diagram for ferromagnetic-antiferromagnetic transitions of a three-electron QD for two values of an applied field: $\Omega_c = \omega_c/\omega_0 = 0.4$ [black squares refer to the states (1)] and $\Omega_c = \omega_c/\omega_0 = 1.9$ [red circles refer to the states (2)]. Here $\lambda_c = l_0/a_0^*$ and l_0 is the size of the QD potential; R_{Mn} is the position of a Mn atom. The parameters ω_c and ω_0 are the cyclotron frequency and the oscillator frequency of a parabolic potential of a QD, respectively. (b) An example of calculated electron-density distribution in a QD with a single Mn atom and three electrons; a Mn atom is shown as a white cross. We can see strong spatial correlations caused by the Mn–electron exchange interaction, Zeeman energies, and electron–electron repulsion. Reproduced from Ref. [32].

due to the Pauli principle. Since QDs in Ref. [18] did not have the cylindrical symmetry and the Coulomb interaction, the shell-filling effect and Hund's rule were not important. QDs with many carriers and a weak confinement can also be treated using the Thomas–Fermi model [23]; in this model, a many-electron QD becomes split into paramagnetic and ferromagnetic phases [23].

Exact diagonalization calculations for few electrons and a single Mn impurity in a QD can be performed [21,25]. Interesting finding of these studies is that an energy structure of a QD strongly depends on a position of a single Mn impurity. The total Mn–electron interaction energy, which plays a role of a magnetic-polaron binding energy, oscillates again with the number of electrons in a QD due to the shell-filling effect. However, the character of oscillations strongly depends on a position of a Mn atom inside a QD. This reflects a mesoscopic character of the system. Application of an external magnetic field brings additional features into the spectrum and phase diagram [32]. The competition between the Zeeman energies, electron–electron interaction, and Mn–electron exchange coupling creates ferromagnetic and antiferromagnetic phases and a non-trivial phase diagram (Fig. 15). We note that an electron and a Mn spin may have g-factors of opposite signs [32]; this leads to a competition between two Zeeman energies. Few-Mn

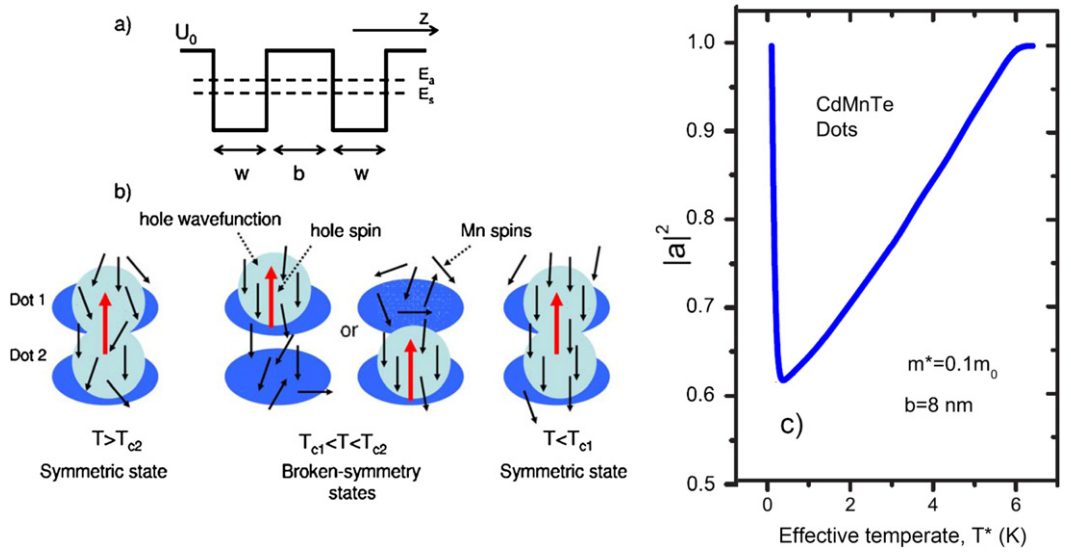

Fig. 16. (a) The QD potential in the z-direction. (b) Schematics of the magnetic QD molecule and three magnetic-polaron phases with a single hole. (c) The asymmetry parameter $|a|^2$ as a function of an effective temperature $T^* = T + T_0$. This graph shows appearance of the broken-symmetry phase with $|a|^2 < 1$. Adopted from Ref. [30].

system in a singly-charged QD ($N = 1$) can also be solved using the exact diagonalization method [34]. If Mn atoms with a short-range interaction form a cluster, a Mn-QD system undergoes a series of magnetic phase transitions from antiferromagnetism to ferromagnetism, with decreasing size of QD [34]. Another important topic to investigate is intra-band spectroscopic signatures of the Mn–electron states in QDs. As was demonstrated theoretically in Ref. [29], the exchange interaction between an electron and Mn atoms brings additional lines in the FIR spectrum at small magnetic fields. Experimentally, such measurements remain quite a challenge.

4. Double quantum dot system: magnetic polarons and spontaneous symmetry breaking

So far, we discussed electronic and magnetic states in single QDs. Now we briefly consider a problem of a QD molecule. Its confining potential has two minima and this may introduce additional phase transitions in the presence of Mn impurities [30]. The QD potential is now in the form: $U_{\rm h}^{\rm QD}(r) = U_0(z) + v_{\rm h}^{\rm QD}(x, y)$, where $U_0(z)$ is double-well potential shown in Fig. 16(a). The simplest case concerns a single hole. To solve for the "ground" state at a finite temperature (i.e. for the lowest-energy state), we employ the free-energy functional and use a variational wave function [30]

$$\Psi_{\rm G} = a\phi_{\rm s} + \sqrt{1 - a^2}\phi_{\rm a},$$

where $\phi_{s(a)}$ are the bound symmetric and asymmetric orbitals of the double-well potential. Unbound states can be included via a perturbation theory [30]. The numerical minimization procedure for the free energy $F(\Psi_{\rm G})$ yields the values of a. If $a = 1$, the ground state is a symmetric orbital, like in undoped QD molecule or in hydrogen molecule ion H_2^-. If the mathematics gives $a < 1$, we deal with an asymmetric state which is quite different to the usual symmetric ground-state orbital. The case $a < 1$ would manifest a formation of a broken-symmetry magnetic-polaron state. Indeed, we observed the states with broken spatial symmetry (Fig. 16 (b) and (c)). If the Mn–hole interaction is strong enough, the hole wave functions tends to be localized in one of the wells; the physical reason is that any localization in a magnetic semiconductor lowers a total magnetic-exchange energy. A simple condition for the formation of broken-symmetry polaron states in a QD molecule is $\Delta_{\rm tun} \sim E_{\rm Mn-h,binding}$, where $E_{\rm Mn-h,binding}$ is the total Mn–hole interaction energy (magnetic-polaron binding energy) and $\Delta_{\rm tun}$ is the tunnel splitting between the symmetric and antisymmetric single-particle levels in a double-well potential of a QD. The calculated phase diagram is quite interesting [30]. With decreasing temperature, the ground state changes from the normal symmetric state to a state with spontaneously broken symmetry. The symmetry of a magnetic molecule is recovered at very low temperatures

(Fig. 16(c)). Overall, we found that a double quantum-dot system made of diluted magnetic semiconductor behaves unlike the usual molecules where the ground state is always a symmetric orbital. It could be that more sophisticated computational methods can give a more complex phase diagram for a magnetic QD molecule. The paper [30] also suggests that a magnetic double QD with broken-symmetry phases can be used as a voltage-controlled nanoscale memory cell: two states with broken symmetry (Fig. 16(b)) can play a role of a bit.

Acknowledgements

The author acknowledges helpful discussions with Henri Mariette, L. Besombes, Pierre Petroff, Bruce McCombe, Leigh Smith, Sebastian Mackowski, Richard Warburton, and Paul Koenraad.

References

[1] L. Besombes, Y. Leger, L. Maingault, D. Ferrand, H. Mariette, J. Cibert, Phys. Rev. Lett. 93 (2004) 207403.
[2] L. Besombes, Y. Leger, L. Maingault, D. Ferrand, H. Mariette, J. Cibert, Phys. Rev. B 71 (2005) 161307(R).
[3] Y. Léger, L. Besombes, J. Fernández-Rossier, L. Maingault, H. Mariette, Phys. Rev. Lett. 97 (2006) 107401.
[4] A. Kudelski, A. Lemaitre, A. Miard, P. Voisin, T.C.M. Graham, R.J. Warburton, O. Krebs, Phys. Rev. Lett. 99 (2007) 247209.
[5] J. Seufert, G. Bacher, M. Scheibner, A. Forchel, S. Lee, M. Dobrowolska, J.K. Furdyna, Phys. Rev. Lett. 88 (2001) 027402.
[6] P.S. Dorozhkin, A.V. Chernenko, V.D. Kulakovskii, A.S. Brichkin, A.A. Maksimov, H. Schoemig, G. Bacher, A. Forchel, S. Lee, M. Dobrowolska, J.K. Furdyna, Phys. Rev. B 68 (2003) 195313.
[7] S. Mackowski, T. Gurung, T.A. Nguyen, H.E. Jackson, L.M. Smith, G. Karczewski, J. Kossut, Appl. Phys. Lett. 84 (2004) 3337.
[8] S. Mackowski, T. Gurung, H.E. Jackson, L.M. Smith, G. Karczewski, J. Kossut, Appl. Phys. Lett. 87 (2005) 072502.
[9] C. Gould, A. Slobodskyy, D. Supp, T. Slobodskyy, P. Grabs, P. Hawrylak, F. Qu, G. Schmidt, L.W. Molenkamp, Phys. Rev. Lett. 97 (2006) 017202.
[10] T. Gurung, S. Mackowski, G. Karczewski, H.E. Jackson, L.M. Smith, Appl. Phys. Lett. 93 (2008) 153114.
[11] R. Beaulac, P.I. Archer, D.R. Gamelin, J. Solid State Chem. 181 (2008) 1582–1589.
[12] D.J. Norris, N. Yao, F.T. Charnock, T.A. Kennedy, Nano Lett. 1 (2001) 3;
J.F. Suyver, S.F. Wuister, J.J. Kelly, A. Meijerink, Phys. Chem. Chem. Phys. 2 (2000) 5445–5448.
[13] A.K. Bhattacharjee, C. Benoit à la Guillaume, Phys. Rev. B 55 (1997) 10613.
[14] A.L. Efros, M. Rosen, E.I. Rashba, Phys. Rev. Lett. 87 (2001) 206601.
[15] A.K. Bhattacharjee, J. Perez-Conde, Phys. Rev. B 68 (2003) 045303.
[16] K. Chang, S.S. Li, J.B. Xia, F.M. Peeters, Phys. Rev. B 69 (2004) 235203.
[17] A.O. Govorov, Phys. Rev. B 70 (2004) 035321.
[18] J. Fernandez-Rossier, L. Brey, Phys. Rev. Lett. 93 (2004) 117201.
[19] A.O. Govorov, A.V. Kalameitsev, Phys. Rev. B 71 (2005) 035338.
[20] A.O. Govorov, Phys. Rev. B 72 (2005) 075359.
[21] F. Qu, P. Hawrylak, Phys. Rev. Lett. 95 (2005) 217206.
[22] S.-J. Cheng, Phys. Rev. B 72 (2005) 235332.
[23] A.O. Govorov, Phys. Rev. B 72 (2005) 075358.
[24] J.I. Climente, M. Korkusinski, P. Hawrylak, J. Planelles, Phys. Rev. B 71 (2005) 125321.
[25] N.T.T. Nguyen, F.M. Peeters, Phys. Rev. B 76 (2007) 045315.
[26] J. Fernández-Rossier, Phys. Rev. B 73 (2006) 045301.
[27] R.M. Abolfath, P. Hawrylak, I. Zutic, Phys. Rev. Lett. 98 (2007) 207203.
[28] R. Abolfath, P. Hawrylak, I. Zutic, New J. Phys. 9 (2007) 353.
[29] I. Savic, N. Vukmirovic, Phys. Rev. B 76 (2007) 245307.
[30] W. Zhang, T. Dong, A.O. Govorov, Phys. Rev. B 76 (2007) 075319.
[31] M.M. Glazov, E.L. Ivchenko, L. Besombes, Y. Léger, L. Maingault, H. Mariette, Phys. Rev. B 75 (2007) 205313.
[32] N.T.T. Nguyen, F.M. Peeters, Phys. Rev. B 78 (2008) 045321.
[33] F. Qu, P. Vasilopoulos, Phys. Rev. B 74 (2006) 245308;
M. Tolea, B.R. Bulka, Phys. Rev. B 75 (2007) 125301.
[34] S.-J. Cheng, Phys. Rev. 77 (2008) 115310.
[35] A.Kh. Manaselyan, A.V. Ghazaryan, A.A. Kirakosyan, J. Contemp. Phys. (Armenian Academy of Sciences) 43 (2008) 211.
[36] J. van Bree, P. Koenraad, J. Fernandez-Rossier, Phys. Rev. B 78 (2008) 165414.
[37] N. Lebedeva, H. Holmberg, P. Kuivalainen, Phys. Rev. B 77 (2008) 245308.
[38] C. Zener, Phys. Rev. 81 (1950) 440;
M.A. Ruderman, C. Kittel, Phys. Rev. 96 (1954) 99.
[39] Y.D. Park, A.T. Hanbicki, S.C. Erwin, C.S. Hellberg, J.M. Sullivan, J.E. Mattson, T.F. Ambrose, A. Wilson, G. Spanos, B.T. Jonker, Science 295 (2002) 651.
[40] H. Drexler, D. Leonard, W. Hansen, J.P. Kotthaus, P.M. Petroff, Phys. Rev. Lett. 73 (1994) 2252.

[41] J. Warnock, P.A. Wolff, Phys. Rev. B 31 (1985) 6579;
A.K. Bhattacharjee, Phys. Rev. B 35 (1987) 9108.
[42] I.Y. Karlik, I.A. Merkulov, D.N. Mirlin, L.P. Nikitin, V.I. Perel, V.F. Sapega, Fiz. Tverd. Tela (Leningrad) 24 (1982) 3550, Sov. Phys. Solid State 24 (1982) 2022;
J.M. Kikkawa, J.J. Baumberg, D.D. Awschalom, D. Leonard, P.M. Petroff, Phys. Rev. B 50 (1994) 2003.
[43] J.K. Furdyna, J. Appl. Phys. 65 (1988) 29.
[44] E.L. Ivchenko, G.E. Pikus, Superlattices and Other Heterostructures. Symmetry and Optical Phenomena, Springer, Berlin, 1997.
[45] M. Bayer, A. Kuther, A. Forchel, A. Gorbunov, V.B. Timofeev, F. Schafer, J.P. Reithmaier, T.L. Reinecke, S.N. Walck, Phys. Rev. Lett. 82 (1999) 1748.
[46] J.-Y. Marzin, J.-M. Gerard, A. Izrael, D. Barrier, G. Bastard, Phys. Rev. Lett. 73 (1994) 716.
[47] A. Hogele, S. Seidl, M. Kroner, K. Karrai, R.J. Warburton, B.D. Gerardot, P.M. Petroff, Phys. Rev. Lett. 93 (2004) 217401.
[48] M. Kroner, A.O. Govorov, S. Remi, B. Biedermann, S. Seidl, A. Badolato, P.M. Petroff, W. Zhang, R. Barbour, B.D. Gerardot, R.J. Warburton, K. Karrai, Nature (London) 451 (2008) 311.
[49] A.K. Bhattacharjee, C. Benoit a la Guillaume, Solid State Commun. 113 (2000) 17.
[50] S.-S. Li, J.-B. Xia, Nanoscale Res. Lett. 2 (2007) 554.
[51] C. Riva, R.A. Escorcia, A.O. Govorov, F.M. Peeters, Phys. Rev. B 69 (2004) 245306.
[52] L. Besombes, Y. Leger, J. Bernos, H. Boukari, H. Mariette, J. Fernandez-Rossier, R. Aguado, Phys. Rev. B 78 (2008) 125324.
[53] D. Scalbert, J. Cernogora, C. Benoit la Guillaume, Solid State Commun. 66 (1988) 571.
[54] J.M. Smith, P.A. Dalgarno, R.J. Warburton, K. Karrai, B.D. Gerardot, P.M. Petroff, Phys. Rev. Lett. 94 (2005) 197402.
[55] C. Benoit a la Guillaume, Yu.G. Semenov, M. Combescot, Phys. Rev. B 51 (1995) 14124.
[56] J.-W. Wu, A.V. Nurmikko, J.J. Quinn, Phys. Rev. B 34 (1986) 1080.